



Laser ablation-assisted synthesis of tungsten sub-oxide (W₁₇O₄₇) nanoparticles in water: effect of laser fluence

Zohreh Famili¹ · Davoud Dorrnian¹ · Amir Hossein Sari¹

Received: 23 January 2020 / Accepted: 26 May 2020 / Published online: 2 June 2020
© Springer Science+Business Media, LLC, part of Springer Nature 2020

Abstract

Tungsten sub-oxide (W₁₇O₄₇) nanoparticles were produced for the first time, via pulsed laser ablation of a pure tungsten target in distilled water. The beam of a Q-switched Nd:YAG laser of 1064 nm wavelength with 0.6, 0.8, 1.2 and 1.4 J/cm² fluences was employed to irradiate the target. Produced nanoparticles were characterized using field emission scanning electron microscopy coupled with energy dispersive spectrometry, transmission electron microscopy, Fourier transform infrared spectroscopy, X-ray diffraction (XRD), UV–Vis absorption spectroscopy and room temperature Photoluminescence (PL). XRD patterns revealed that all samples possess the monoclinic structure corresponding to W₁₇O₄₇ phase. With increasing the laser fluence, the average size of the nanoparticles increased and subsequently, their band gap energy decreased. The PL spectra of the samples show the presence of oxygen vacancies or defects.

Keywords Tungsten oxide nanoparticles · Tungsten sub-oxide · Laser ablation · Exciton absorption

1 Introduction

In the first two decades of the recent century, nanoscience and nanotechnology have had one of the highest rates of growth among all sciences. Nanoscale materials in the forms of insulators, semiconductors and conductors have different morphologies such as particles, tubes, and thin films (Mostafa et al. 2019; Dwivedi et al. 2012, 2013, 2014; Sekhon et al. 2013a; Dorrnian et al. 2012; Zamiranvari et al. 2017; Alaei et al. 2012; Isaac et al. 2016). Researches and activities in nanomaterials can be categorized in three fields of nanomaterials synthesizing, properties and applications (Sekhon et al. 2013b; Dwivedi et al. 2011a, 2015; Ghasemi and Jafari 2017; Moradi et al. 2016).

Recently, transition metal oxide nanostructures have been used in extensive domains such as superconductivity, piezoelectricity, catalysis, microelectronics, ceramics, medical science, coating technology, electronics, cosmetics, colossal magneto-resistance

✉ Davoud Dorrnian
doran@srbiau.ac.ir

¹ Laser Lab., Plasma Physics Research Center, Science and Research Branch, Islamic Azad University, Tehran, Iran

effect and so on (Solati and Dorranian 2016a; Kim et al. 2016; Kumar and Mohanta 2011). Among them, tungsten oxide as an indirect and wide gap semiconductor has unique electrical, gasochromic and photoelectrochromic properties so that can be used in infrared switching devices, non-emissive displays, photovoltaic organic solar cells, large area displays, photocatalysis, gas and chemical sensors, biosensors, supercapacitors, information storage media, optical modulators, rearview mirrors in cars, windows with adjustable light transmission, anti-glare mirrors and the like (Isaac et al. 2016; Kim et al. 2016; Kumar and Mohanta 2011; Barreca et al. 2011; Chala et al. 2017; He and Yao 2007; Lavanya et al. 2017; Popov et al. 2018; Wang et al. 2017; Yamazaki et al. 2018; Ragunathan et al. 2015; Wasmı et al. 2014).

Tungsten oxides possess various phases and compositions that can be classified into stoichiometric (WO_3 and WO_2) and non-stoichiometric ($\text{W}_{24}\text{O}_{64}$, $\text{W}_{18}\text{O}_{49}$ and etc.) structures (Kim et al. 2016; Ragunathan et al. 2015; Wasmı et al. 2014; Fukushi et al. 2017; Ishida et al. 2017; Zhan et al. 2018; Zhao et al. 2019). Tungsten oxides received considerable attention due to their abundance, highly tunable composition, non-toxicity, and high chemical stability (Lavanya et al. 2017; Ishida et al. 2017; Fakhari et al. 2018a). Tungsten sub-oxide (WO_{3-x}) nanostructures because of the tunable localized surface Plasmon resonance (LSPR) effect exhibit the strong absorptions in the near-infrared (NIR) region (Chala et al. 2017; Zhao et al. 2019). Thus from the perspective of energy saving, they are very supernatural candidates for photothermal applications, solar collectors, solar devices, transparent smart windows and optical filters (Chala et al. 2017; Zhao et al. 2019; Guo et al. 2012). Also, it has been found that WO_{3-x} nanowires are effective EM wave absorbing owing to their high dielectric properties (Wang et al. 2017).

The properties of prepared nanostructures depend on their microstructure and growth form (Zhan et al. 2018). It has been observed the size of the WO_3 particles changes the band gap and band bending at the interfaces (Barreca et al. 2011). There are many reports that show band gap of bulk tungsten oxides depending on morphology and stoichiometry can be between 2.6 and 3.4 eV (Zhao et al. 2019; Brütsh et al. 2017). Of course for tungsten oxides nanoparticles, band gaps have been reported up to 4.2 eV (Brütsh et al. 2017; Cong et al. 2014). Because of the quantum confinement effect, WO_{3-x} nanoparticles with small sizes (generally < 10 nm) exhibit supernatural optical and electronic properties hence, they can be utilized in novel light energy conversion equipment and sensing systems (Wang et al. 2017; Zhan et al. 2018).

There are various methods to produce tungsten oxide nanostructures, such as laser pyrolysis, sputtering, chemical vapor deposition, hydrothermal, sol-gel deposition, electrical arc discharge, acid precipitation and pulse laser ablation in liquid and gas. Laser ablation in liquid (LAL) is a facile, fast, clean and cheap method. Contrary to other wet chemical approaches, LAL is known as a green chemistry technique for producing high purity, uniformity and homogeneity metal and metal oxide nanostructures in colloidal phase without any unnecessary byproducts and toxic chemical precursors. In addition, the composition of the NPs is firmly controlled by the primary materials of the liquid. One of the advantages of LAL method is that the NPs produced have a narrow size distribution. Because nanoparticles with homogeneous nucleation can be saturated where saturation quickly leads to the reduction of particles to smaller sizes in the colloid (Alaei et al. 2012; Ghasemi and Jafari 2017; Barreca et al. 2011; Fakhari et al. 2018a,b; Solati and Dorranian 2015,2016b; Shah et al. 2009; Mansoureh and Parisa 2018; Supothina et al. 2007).

In this method, there are many parameters concerning the source (such as laser wavelength, laser fluence, repetition rate) and the liquid environment (such as composition,

viscosity, dipole moment and dielectric constant) controlling the morphology of the synthesized nanostructures (Barreca et al. 2011; Solati and Dorrnian 2016b).

In this paper, we produce tungsten sub-oxide ($W_{17}O_{47}$) nanoparticles in distilled water from a pure tungsten target in order to investigate the effect of the laser fluence on the properties of the produced nanoparticles. According to the authors' studies, there is only one report about the synthesis of tungsten sub-oxide ($WO_{2.9}$) nanoparticles by laser ablation in water (Barreca et al. 2011) and our work is the first report on the synthesis of tungsten sub-oxide ($W_{17}O_{47}$) nanoparticles by laser ablation in water.

2 Experimental

Tungsten oxide nanoparticles were produced by pulsed laser ablation of a tungsten plate (99.9%) in distilled water. The tungsten target was a circular plate with 2 mm thickness and 5 cm diameter. The target and containers were cleaned ultrasonically in alcohol, acetone, and deionized water before the experiments. Tungsten plate was placed on the bottom of a glass vessel containing 50 ml of distilled water, such that the height of the liquid above the tungsten surface was about 10 mm.

The plate surface was irradiated vertically with 1064 nm wavelength of a pulsed Nd:YAG laser. The pulse repetition rate and the pulse width were 10 Hz and 7 ns respectively. The laser beam diameter was 6 mm, which was focused on the surface of W target by an 80 mm focal length convex lens. Laser fluences were 0.6, 0.8, 1.2, and 1.4 J/cm² before the lens. During laser irradiation, the target was moved by using a rotational or x–y motion stage to prevent laser pulses from irradiating the same spot.

The following analytical techniques were applied for the characterization of the prepared samples. Morphology studies and elemental characterizations were carried out using field emission scanning electron microscope (FESEM; TESCAN MIRA3) coupled with energy dispersive spectrometry (EDS). Transmission electron microscopy (TEM) images were taken by Zeiss-EM10C-100 kV microscope. The fourier transform infrared (FTIR) spectra of samples were recorded using Perkin–Elmer FTIR spectrometer (Spectrum Two) in the range of 450–4000 cm⁻¹. X-ray diffraction (XRD) patterns of the products were Prepared using PANalytical-X'Pert PRO X-ray diffractometer with Cu K α radiation ($\lambda = 0.1514060$ nm). UV–Vis–NIR absorption spectroscopy was performed by means of a PerkinElmer Lambda 950 spectrometer in the range 200–1100 nm. The photoluminescence (PL) spectra of the samples were obtained using a Fluorescence Spectrophotometer F-4500.

3 Results and discussion

3.1 EDS-FESEM analysis

For EDS-FESEM analysis, few drops of suspensions were dried on silicon substrates at room temperature. The EDS analysis was accomplished to investigate the elemental composition of the samples. Figure 1 shows the EDS spectra of the samples prepared at different laser fluences. The EDS spectra reveal that there are only W and O elements in the samples. The very high W peak observed in the EDS spectra may be due to the superposition of the X-ray emission $W M_{\alpha_1}$ line with $Si K_{\alpha_{1,2}}$ line from the silicon substrate (Guo et al. 2012).

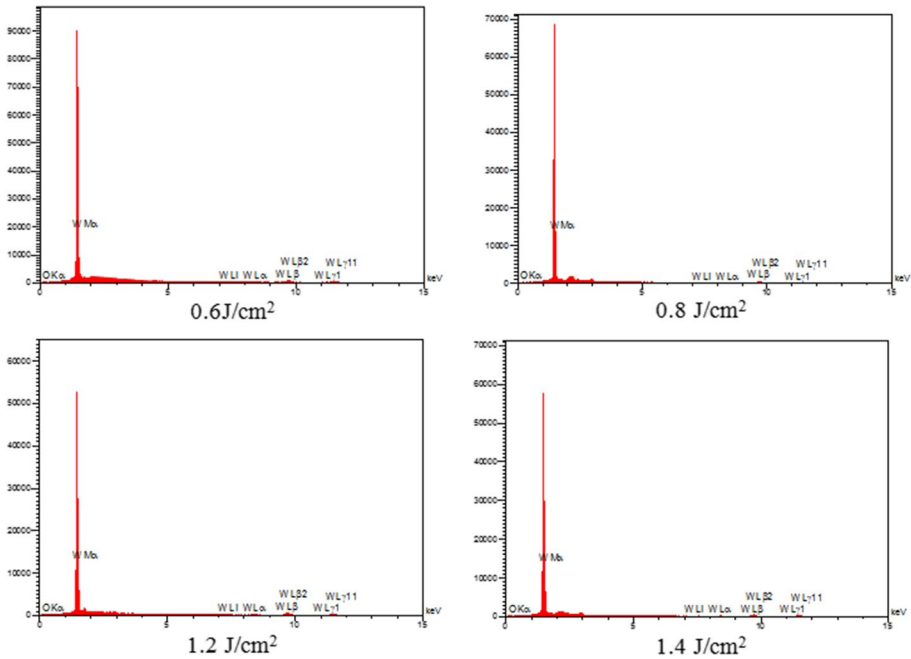


Fig. 1 EDS spectra of samples prepared at different laser fluences

The morphology of the tungsten oxide nanoparticles was investigated by FESEM. The FESEM images of the tungsten oxide nanoparticles prepared by laser ablation in the water at different laser fluences are shown in Fig. 2. It can be seen that nanoparticles are spherical and adhered to each other. It is also seen that the agglomerations formed in samples prepared at 0.6 and 0.8 J/cm² laser fluence are spherical while in samples prepared at 1.2 and 1.4 J/cm² laser fluence are conical.

3.2 TEM analysis

The TEM analysis was performed for further investigation of morphologies and size distributions of samples prepared at different fluences. TEM images of the nanoparticles on the scale of 250 nm are shown in Fig. 3. TEM images reveal the formation of the almost spherical nanoparticles in samples prepared at laser fluences of 0.6, 0.8, 1.2 and 1.4 J/cm².

Size distribution histograms of nanoparticles were plotted using ImageJ software (by counting particles on several images obtained on different areas on the grid). According to the histograms plotted in Fig. 4, the average particle size of the samples prepared at 0.6, 0.8, 1.2 and 1.4 J/cm² laser fluence are calculated about 41.62, 43.24, 51.38 and 53.88 nm, respectively (Table 1). Consequently, with increasing the laser fluence, the average particle size is increased which is in agreement with previous reports of others (Barreca et al. 2011; Fakhari et al. 2018a,b).

K. Yahiaoui. et al. showed in the pulsed laser ablation process of a target, there are two kinds of ablation process: at low laser intensity, normal surface evaporation and at laser intensity higher than the threshold laser intensity, phase explosion process occurs.

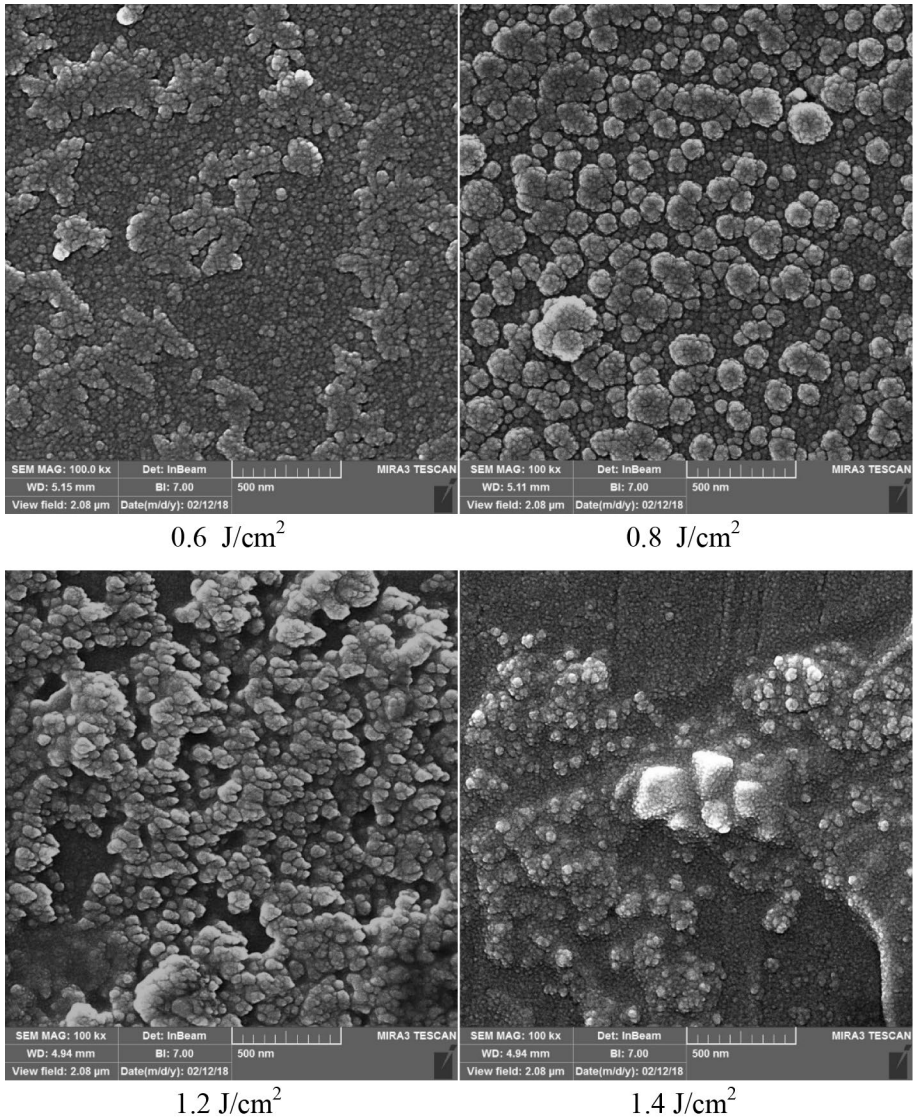


Fig. 2 FESEM images of $W_{17}O_{47}$ nanoparticles prepared at different laser fluences

In their work, the threshold laser intensity for the phase explosion process of tungsten is reported 6×10^{10} W/cm² (Yahiaoui et al. 2010). The pulse width in our experiment is 7 ns hence threshold laser fluence for phase explosion process of tungsten is 420 J/cm². Therefore, in our work, the surface evaporation process happens. In this case, with the increase in laser fluence, nanoparticles size increases. Increment of the average particle size with increasing the laser fluence is because of the formation of plasma bubbles with higher material content and longer lifetime (Fakhari et al. 2018b).

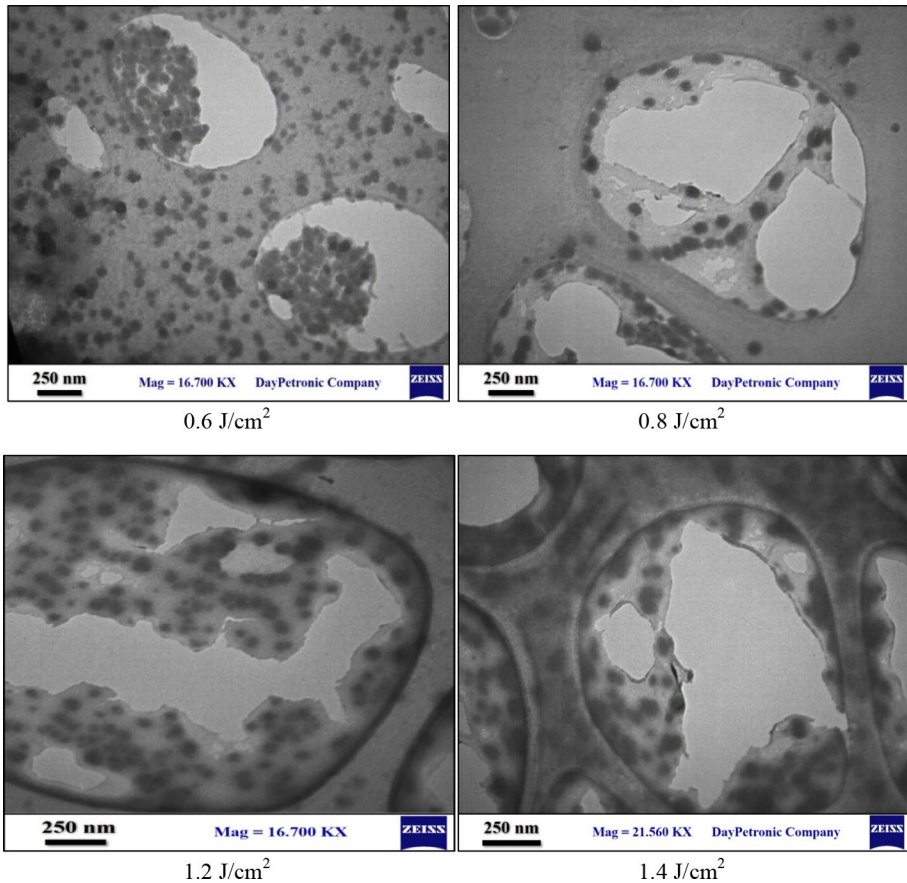


Fig. 3 TEM images of $W_{17}O_{47}$ nanoparticles prepared at different laser fluences

In order to compare of the size distribution of the samples, the standard deviations of particles size in graphs relevant to 0.6, 0.8, 1.2 and 1.4 J/cm^2 laser fluences were computed and values of 11.84, 12.71, 14.52 and 17.08 nm were obtained, respectively (Table 1). As a result, in prepared samples at lower laser fluences, the size distribution is narrower which confirms the formation of more uniform particles in lower laser fluences.

3.3 FTIR studies

The FTIR spectra were recorded in the spectral range of 450–4000 cm^{-1} . The FTIR spectra of tungsten oxide nanoparticles prepared by laser pulses at different laser fluences in distilled water are shown in Fig. 5. The strong and broad absorption peaks at 3451, 3433, 3437 and 3433 cm^{-1} wavenumbers are ascribed to the stretching modes of OH groups. The medium and broad peaks at 1637 cm^{-1} and the low-intensity peaks located at 1385 cm^{-1} are due to bending modes of water molecules (Fakhari et al. 2018a; Bishop et al. 1994; Chong et al. 2004; Daniel et al. 1987; Gotić et al. 2000; Petit and Puskar 2018; Petit et al. 2017; Shenderova et al. 2011; Stehlik et al. 2016; Tiwari and Gong 2008).

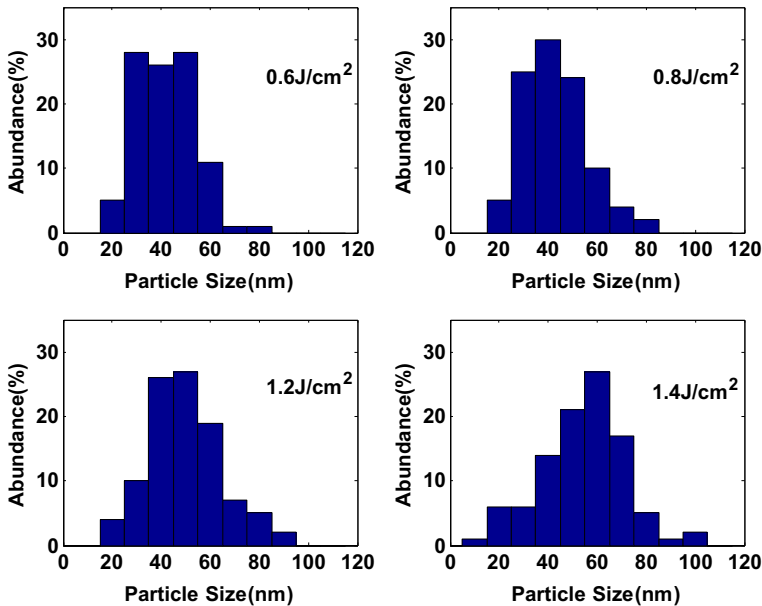


Fig. 4 Size distributions of nanoparticles prepared at different laser fluences. Data are extracted from TEM images

Table.1 Size distributions and band gap energies of samples prepared at laser fluences.

Laser fluence (J/cm^2)	0.6	0.8	1.2	1.4
Crystallite size (nm) (Scherrer formula)	10.51	11.20	12.51	12.83
Average size of Nanoparticles (nm) (TEM images)	41.62	43.24	51.38	53.88
Standard deviation (nm)	11.84	12.71	14.52	17.08
Band gap energy (eV) for $m = 1/2$	5.86	5.84	5.68	5.66
Band gap energy (eV) for $m = 2$	5.68	5.65	5.26	5.24

The bands in the region of $600\text{--}780\text{ cm}^{-1}$ correspond to the stretching modes of bridging oxygen, $\nu(\text{O}\text{--}\text{W}\text{--}\text{O})$ which imply the existence of the bonds between oxygen and tungsten particles in samples (Zamiranvari et al. 2017; Dwivedi et al. 2012; Alaei et al. 2012; Isaac et al. 2016; Sekhon et al. 2013b). At laser fluences of 0.6, 0.8, 1.2 and 1.4 J/cm^2 , these characteristic peaks are at 618, 638, 662 and 662 cm^{-1} wavenumbers, respectively. The increment of wavenumbers for the stretching vibration mode of $\nu(\text{O}\text{--}\text{W}\text{--}\text{O})$ with increasing the laser fluence is ascribed to the increase in the interplanar distance and the lengths of $\text{O}\text{--}\text{W}\text{--}\text{O}$ bonds which confirms the existence of surface oxygen vacancies on tungsten oxide (Fakhari et al. 2018a). The electronic band structures of prepared nanoparticles strongly influence by these oxygen vacancies, which will be discussed in Sect. 3.6.

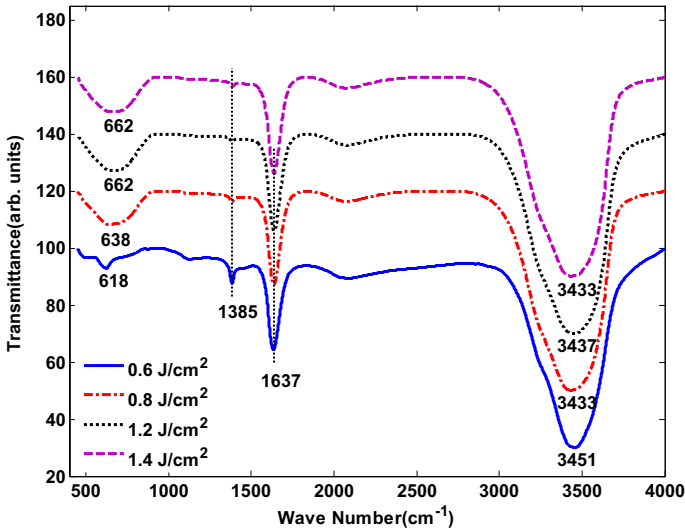


Fig. 5 FTIR spectra of samples prepared at different laser fluences

3.4 XRD results

XRD studies were performed to investigate the crystal structure and preferred orientation of the crystallites. For XRD characterization, several droplets of the transparent colloidal samples prepared at different laser fluences were placed on the silicon substrate with dimensions of 1 cm × 1 cm and 1 mm thick and dried naturally at room temperature. The XRD patterns of the samples prepared at laser fluences of 0.6, 0.8, 1.2 and 1.4 J/cm² and W target are presented in Fig. 6. It is observed that the XRD peaks of samples occur at similar angles and are different from W target peaks. It can be deduced that chemical and physical processes occurred between the ablated W and water molecules, which caused the formation of tungsten oxide nanoparticles in the water environment (Fakhari et al. 2018a; Solati and Dorrani 2016b).

The XRD patterns at laser fluences of 0.6 and 0.8 J/cm² show XRD peaks at 2θ values of 16.19° and 43.79° corresponding to lattice reflection planes (102) and (115) of monoclinic W₁₇O₄₇ phase (PDF: 01-079-0171), respectively. The broadening of the XRD peaks of these samples suggests that the films are not crystallized fully and are partly amorphous in nature.

At laser fluences of 1.2 and 1.4 J/cm², monoclinic phase W₁₇O₄₇ (PDF: 01-079-0171) became more prominent with the evolution of new peaks at 2θ values of 13.49°, 25.04° and 37.78° corresponding to lattice reflection planes (201), (111) and (610) with a strong preferential growth along (102) plane. The XRD patterns at different laser fluences show the intensity of the peaks increases with increasing of laser fluence, indicating increased crystallinity. The crystallite size is determined using the Scherrer formula (Cullity and Stock 2014):

$$D = k\lambda/(\beta \cos \theta) \quad (1)$$

where k is constant ($0.89 < k < 1$) varies with Miller indices and crystallite shape but usually nearly equal to 0.94, λ is X-ray wavelength, β is the full width at the half maximum

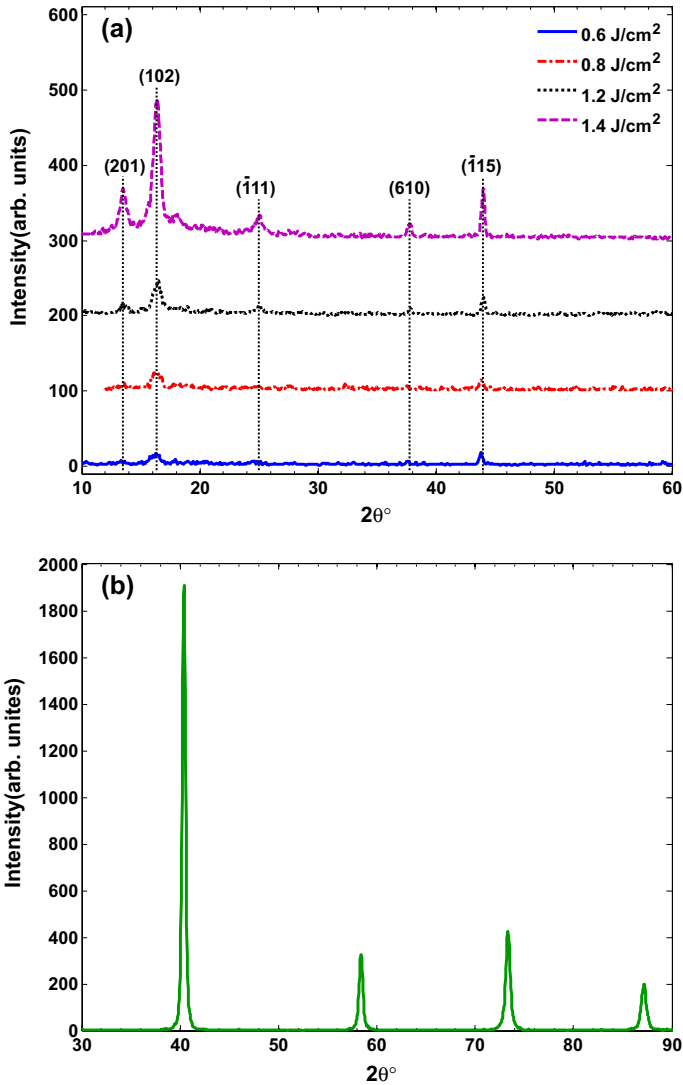


Fig. 6 XRD patterns of **a** tungsten oxide nanoparticles at different laser fluences and **b** tungsten target

(FWHM) of the dominant diffraction peak in radian, and θ is the diffraction angle. The dependence of crystallite size on laser fluence is indicated in Table 1. It is seen that with increasing laser fluence from 0.6 to 1.4 J/cm² the crystallite size increases. The increment of size is in accordance with the results of mentioned in TEM analysis.

Actually there is not any known relation between the laser ablation parameters and tungsten oxide crystalline structure. However, a comparison between Fakhari et al. (Fakhari et al. 2018a) and Barreca et al. (Barreca et al. 2011) reports shows that in the case of high laser fluence i.e. 13–23 J/cm², probability of tungsten trioxide (WO₃)

nanoparticles production is higher while in the range of low laser fluence i.e. 1–5 J/cm², tungsten sub-oxide (WO_{3-x}) will be synthesized.

3.5 UV absorption spectra

The UV–Vis spectra of the colloidal solutions prepared by PLA in water were collected by means of a PerkinElmer Lambda 950 spectrometer in the 200–1100 nm wavelength range with respect to deionized water absorption as the base line using 1 cm × 1 cm quartz cells. The results are presented in Fig. 7. It is imagined a UV absorption peak from the exciton absorption of tungsten oxide nanoparticles at shorter wavelengths than 200 nm. The spectra are characterized by an increasing absorption starting from 400 nm towards shorter wavelengths. It is in agreement with the UV absorption properties of WO₃ (Barreca et al. 2011; He and Yao 2007). Although the absorption features appear the same, the absorbance intensity increases with increasing laser fluence, since the absorbance intensity is directly proportional to the number of particles in suspension, and with increasing laser fluence, the number of prepared particles in suspension increases. FWHM of the excitonic peak of semiconductor nanoparticles directly depends on the width of their size distribution curve. For the case of our produced samples, the FWHM of the excitonic peak was increased with increasing the laser fluence. Because as is shown in Table 1, with increasing the laser fluence, the uniformity of size distribution of the produced nanoparticles was increased.

There is a soft absorption peak at about 265 nm in the absorption spectra of samples which were produced by laser fluences of 1.2 and 1.4 J/cm². This peak is attributed to another morphology of tungsten oxide nanostructures. This peak was firstly reported by Schieder et al. in the absorption spectrum of tungsten oxide nanotubes (Schieder et al. 2013). Results show that with increasing the laser fluence in the procedure of nanostructure production, we may synthesize tungsten oxide nanotubes.

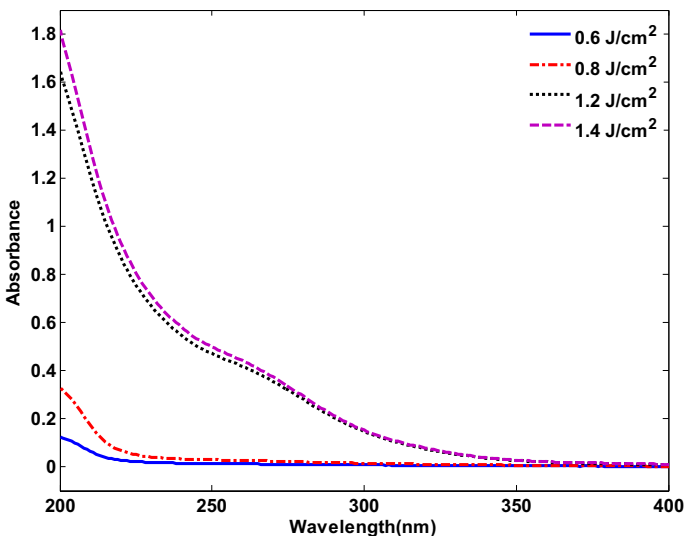


Fig. 7 UV–Vis absorption spectra of samples prepared at different laser fluences

The band gap energy of crystalline semiconductors is calculated by following the Tauc equation (Ghobadi 2013; Viezbicke et al. 2015; Kim et al. 2000; Tauc and Menth 1972; Pankove 2010; Gullapalli et al. 2010; Granqvist 2000; González-Borrero et al. 2010):

$$\alpha h\nu = B(h\nu - E_g)^m \quad (2)$$

where $h\nu$ is incident photon energy, E_g the band gap energy and B a factor that depends on the transition probability and can be supposed to be constant within the optical frequency range; α is the absorption coefficient defined by the Beer-Lambert's law as $\alpha = 2.303 A/d$ and d is the distance between sides of the cell (Ghobadi 2013). Also, m is the index which can have different values of $1/2$, $3/2$, 2 , and more depending on the transitions are direct allowed, direct forbidden, indirect allowed and indirect forbidden transitions, respectively (Ghobadi 2013; Viezbicke et al. 2015; Kim et al. 2000; Granqvist 2000). To calculate the band gap energy $(\alpha h\nu)^{1/m}$ is plotted against $h\nu$ (Fig. 8). There is a distinct linear range in the plot which denotes the onset of absorption. The location on the $h\nu$ axis where the linear section of the curve crosses is the band gap energy (Ghobadi 2013; Viezbicke et al. 2015; Kim et al. 2000; Gullapalli et al. 2010; González-Borrero et al. 2010; Dwivedi et al. 2011b).

Since in tungsten oxide, the top of the valence band is formed by the filled O 2p orbitals, while the bottom of the conduction band is constituted by the empty W 5d orbitals to some ninety percent, the transitions are allowed thus the value of m can be

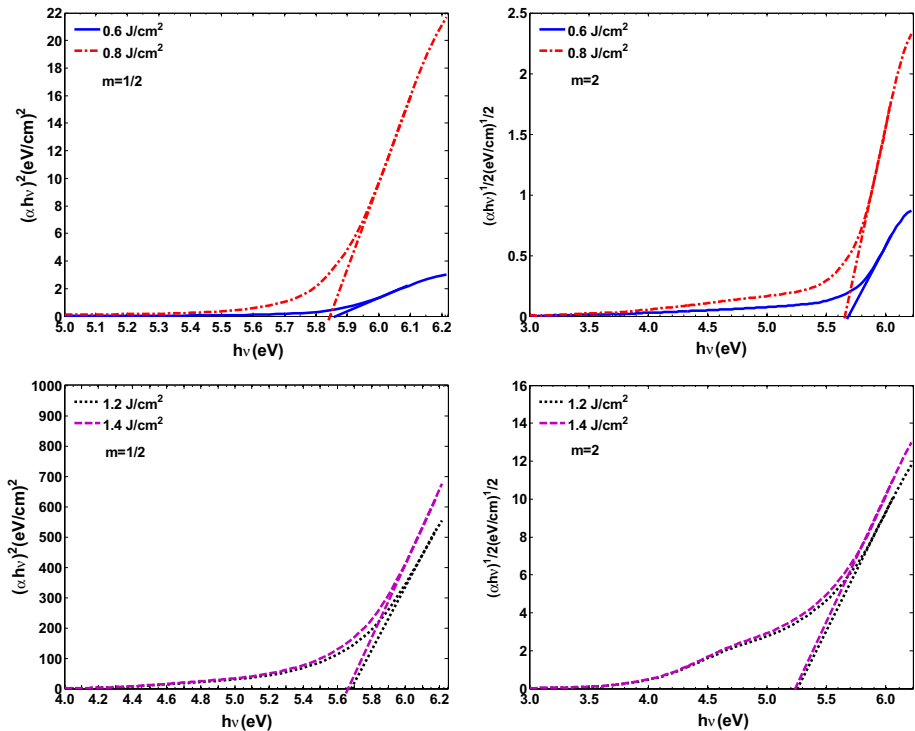


Fig. 8 Plot of $(\alpha h\nu)^m$ versus $h\nu$ for $m=1/2, 2$ corresponding to direct and indirect allowed transitions in samples respectively

1/2 or 2 (Gullapalli et al. 2010; Granqvist 2000; González-Borrero et al. 2010). To determine whether m value is 1/2 or 2, we must check that the graph $(\alpha h\nu)^{1/m}$ versus $h\nu$ for which of these two values represents a better linear fit (Viezbicke et al. 2015). In Fig. 8 it is observed a suitable linear fit for both values of $m=1/2, 2$, corresponding to direct and indirect allowed transitions, respectively.

The values of the band gap energies of samples are presented in Table 1. It is observed that at laser fluences of 0.6, 0.8, 1.2 and 1.4 J/cm², the bandgap energies are 5.86, 5.84, 5.68 and 5.66 eV for $m=1/2$ and 5.68, 5.65, 5.26 and 5.24 eV for $m=2$, respectively, i.e., with increasing the laser fluence, the bandgap energy of tungsten oxide nanoparticles decreases. This result is expected because numerous reports suggest that in nanostructured tungsten oxides, the band gap energy generally decreases with increasing nanostructures size (He and Yao 2007; Gullapalli et al. 2010; Zheng et al. 2011) and on the other hand, results obtained in our TEM and XRD analyses indicate the nanoparticle average size increases with increasing the laser fluence. Of course for tungsten oxides nanoparticles, depending on particle size and synthesis method, band gap energy has been reported up to 4.2 eV (Brütsch et al. 2017; Cong et al. 2014).

The influence of particle size on the band gap can be attributed to the so-called quantum confinement (QC) effect divided into two regimes so-called strong and weak. In strong QC, nanocrystal size is smaller than the Bohr radius, therefore the electron wave functions directly change. This causes the bandgap significantly to modify. While in weak QC, nanocrystal size is larger than the Bohr radius so an indirect perturbation in the electron wave function due to Coulomb effects occurs that causes a relatively smaller shift in the bandgap. Here it can be observed that variations of particle size strongly affect the band gap energies. Thus, it seems strong QC effect has occurred (Gullapalli et al. 2010; Zheng et al. 2011).

3.6 PL emission spectra

The photoluminescence (PL) emission spectra of the samples prepared at different laser fluences are depicted in Fig. 9. PL spectra have been recorded at room temperature under 335 nm excitation wavelengths. As can be seen, in all emission spectra, there is a UV emission with the center wavelength at 375 nm (3.31 eV). With increasing laser fluence from 0.6 to 1.4 J/cm² position of the peak has not changed accordingly the position of the peak is independent of nanoparticles size and band structure. Thus, we suggest that UV emission with the center wavelength at 375 nm might correspond to the presence of oxygen vacancies or defects (Lee et al. 2003). As can be seen, with increasing the laser fluence and subsequent effect i.e. increasing the average size of nanoparticles, PL emission intensity increases because larger nanoparticles would possess more oxygen vacancies or defects (Lee et al. 2003).

By the Tauc method, the band gap energy of samples was obtained equal to 5.66–5.86 eV for $m=1/2$ and 5.24–5.68 eV for $m=2$. These values correspond to photons with wavelengths ranging from 219 to 212 nm for $m=1/2$ and from 237 to 218 nm for $m=2$ while in our PL spectra the wavelength starts from 350 nm, thus, in the PL spectra, there is no emission peak representing the band to band transition. It is observed the presence of an emission band at 525 nm (green emission light) at the laser fluence of 1.4 J/cm². The origin of this band is not clear to us origin is not clear to us.

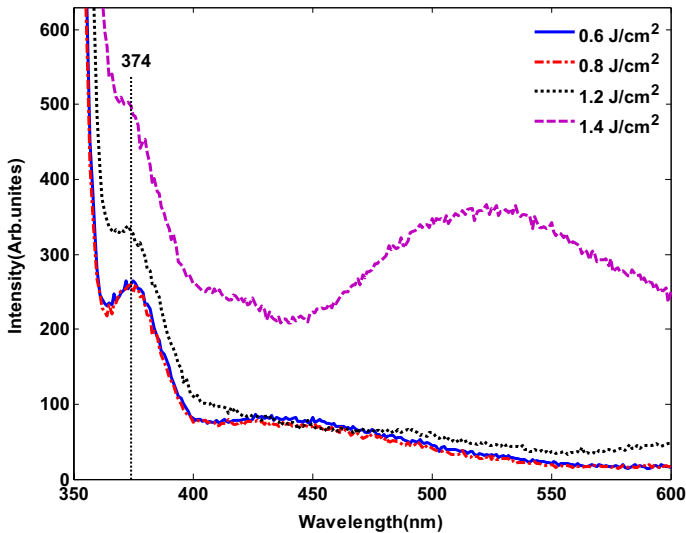


Fig. 9 PL emission spectra of samples prepared at different laser fluences recorded at 335 nm excitation wavelength

4 Conclusion

In this paper, for the first time, we produced $W_{17}O_{47}$ via PLA of a pure tungsten target immersed in distilled water where the vaporization process of the target occurred. Samples were prepared at laser fluencies of 0.6, 0.8, 1.2 and 1.4 J/cm^2 then the effect of laser fluence on products properties was examined. The EDS spectra only confirmed the existence of W and O elements in samples. FESEM images showed the formation of spherical and adhered to each other and consequently the formation of almost spherical and conical agglomerates. TEM images illustrated the average size of nanoparticles increases with increasing laser fluence from 0.6 to 1.4 J/cm^2 . In FTIR spectroscopy characterization peaks at $618\text{--}662\text{ cm}^{-1}$ wavenumber ascribed to the stretching vibration mode of $\nu(O\text{--}W\text{--}O)$ that confirm the existence of the bonds between ablated tungsten and ambient oxygen atoms. The XRD patterns supported the formation of crystallites in monoclinic $W_{17}O_{47}$ phase and the increment of crystallite size with increasing laser fluence using Scherrer formula. Direct and indirect allowed transitions in tungsten oxide nanoparticles were proved using Tauc method and band gap energies were obtained 5.66–5.86 and 5.24–5.68 eV for direct and indirect allowed transitions, respectively. The PL emission spectra showed defects and oxygen vacancies in prepared samples.

References

- Alaei, M., Mahjoub, A.R., Rashidi, A.: Preparation of different WO_3 nanostructures and comparison of their ability for Congo red photo degradation. *Iran J. Chem. Chem. Eng.* **31**, 31–36 (2012)
- Barreca, F., Acacia, N., Spadaro, S., Curro, G., Neri, F.: Tungsten trioxide (WO_3-x) nanoparticles prepared by pulsed laser ablation in water. *Mater. Chem. Phys.* **127**, 197–202 (2011)
- Bishop, J.L., Pieters, C.M., Edwards, J.O.: Infrared spectroscopic analyses on the nature of water in montmorillonite. *Clays Clay Miner.* **42**, 702–716 (1994)

- Brütisch, L., Czolk, J., Popescu, R., Gerthsen, D., Colsmann, A., Feldmann, C.: Surfactant-free synthesis of sub-stoichiometry tungsten oxide nanoparticles and their use as anode buffer layers in organic solar cells. *Solid State Sci.* **69**, 50–55 (2017)
- Chala, T., Wu, C.-M., Chou, M.-H., Gebeyehu, M., Cheng, K.-B.: Highly efficient near infrared photothermal conversion properties of reduced tungsten oxide/polyurethane nanocomposites. *Nanomaterials* **7**, 191 (2017)
- Chong, S., Ingham, B., Tallon, J.: Novel materials based on organic–tungsten oxide hybrid systems I: synthesis and characterisation. *Curr. Appl. Phys.* **4**, 197–201 (2004)
- Cong, S., Tian, Y., Li, Q., Zhao, Z., Geng, F.: Single-crystalline tungsten oxide quantum dots for fast pseudocapacitor and electrochromic applications. *Adv. Mater.* **26**, 4260–4267 (2014)
- Cullity, B.D., Stock, S.R.: *Elements of X-ray Diffraction*, 3rd edn. Pearson, London (2014)
- Daniel, M., Desbat, B., Lassegues, J., Gerand, B., Figlarz, M.: Infrared and Raman study of WO₃ tungsten trioxides and WO₃·xH₂O tungsten trioxide hydrates. *J. Solid State Chem.* **67**, 235–247 (1987)
- Dorranian, D., Solati, E., Dejam, L.: Photoluminescence of ZnO nanoparticles generated by laser ablation in deionized water. *Appl. Phys. A* **109**, 307–314 (2012)
- Dwivedi, N., Kumar, S., Malik, H., Rauthan, C., Panwar, O.: Influence of bonding environment on nanomechanical properties of nitrogen containing hydrogenated amorphous carbon thin films. *Mater. Chem. Phys.* **130**, 775–785 (2011a)
- Dwivedi, N., Kumar, S., Malik, H.K.: Nanostructured titanium/diamond-like carbon multilayer films: deposition, characterization, and applications. *ACS Appl. Mater. Interfaces.* **3**, 4268–4278 (2011b)
- Dwivedi, N., Kumar, S., Tripathi, R., Carey, J., Malik, H.K., Dalai, M.: Structural and electronic characterization of nanocrystalline diamondlike carbon thin films. *ACS Appl. Mater. Interfaces.* **4**, 5309–5316 (2012)
- Dwivedi, N., Kumar, S., Malik, H.K.: Role of base pressure on the structural and nano-mechanical properties of metal/diamond-like carbon bilayers. *Appl. Surf. Sci.* **274**, 282–287 (2013)
- Dwivedi, N., Kumar, S., Rawal, I., Malik, H.K.: Influence of consumed power on structural and nanomechanical properties of nano-structured diamond-like carbon thin films. *Appl. Surf. Sci.* **300**, 141–148 (2014)
- Dwivedi, N., McIntosh, R., Dhand, C., Kumar, S., Malik, H.K., Bhattacharyya, S.: Structurally driven enhancement of resonant tunneling and nanomechanical properties in diamond-like carbon superlattices. *ACS Appl. Mater. Interfaces.* **7**, 20726–20735 (2015)
- Fakhari, M., Torkamany, M.J., Mirnia, S.N., Elahi, S.M.: UV-visible light-induced antibacterial and photocatalytic activity of half harmonic generator WO₃ nanoparticles synthesized by pulsed laser ablation in water. *Opt. Mater.* **85**, 491–499 (2018a)
- Fakhari, M., Torkamany, M.J., Mirnia, S.N.: Linear and nonlinear optical properties of WO₃ nanoparticles synthesized at different fluences of pulsed Nd: YAG laser. *Eur. Phys. J. Appl. Phys.* **84**, 30401 (2018b)
- Fukushi, D., Sasaki, A., Hirabayashi, H., Kitano, M.: Effect of oxygen vacancy in tungsten oxide on the photocatalytic activity for decomposition of organic materials in the gas phase. *Microelectron. Reliab.* **79**, 1–4 (2017)
- Ghasemi, L., Jafari, H.: Morphological characterization of tungsten trioxide nanopowders synthesized by sol–gel modified pechini’s method. *Mater. Res.* **20**, 1713–1721 (2017)
- Ghobadi, N.: Band gap determination using absorption spectrum fitting procedure. *Int. Nano Lett.* **3**, 2 (2013)
- González-Borrero, P., Sato, F., Medina, A., Baesso, M.L., Bento, A.C., Baldissera, G., Persson, C., Niklasson, G.A., Granqvist, C.G., Ferreira da Silva, A.: Optical band-gap determination of nanostructured WO₃ film. *Appl. Phys. Lett.* **96**, 061909 (2010)
- Gotić, M., Ivanda, M., Popović, S., Musić, S.: Synthesis of tungsten trioxide hydrates and their structural properties. *Mater. Sci. Eng., B* **77**, 193–201 (2000)
- Granqvist, C.G.: Electrochromic tungsten oxide films: review of progress 1993–1998. *Sol. Energy Mater. Sol. Cells* **60**, 201–262 (2000)
- Gullapalli, S., Vemuri, R., Ramana, C.: Structural transformation induced changes in the optical properties of nanocrystalline tungsten oxide thin films. *Appl. Phys. Lett.* **96**, 171903 (2010)
- Guo, C., Yin, S., Dong, Q., Sato, T.: The near infrared absorption properties of W₁₈O₄₉. *RSC Adv.* **2**, 5041–5043 (2012)
- He, T., Yao, J.: Photochromic materials based on tungsten oxide. *J. Mater. Chem.* **17**, 4547–4557 (2007)
- Isaac, N.A., Valenti, M., Schmidt-Ott, A., Biskos, G.: Characterization of tungsten oxide thin films produced by spark ablation for NO₂ gas sensing. *ACS Appl. Mater. Interfaces.* **8**, 3933–3939 (2016)
- Ishida, Y., Motono, S., Doshin, W., Tokunaga, T., Tsukamoto, H., Yonezawa, T.: Small nanosized oxygen-deficient tungsten oxide particles: mechanistic investigation with controlled plasma generation in water for their preparation. *ACS Omega* **2**, 5104–5110 (2017)

- Kim, E., Jiang, Z.-T., No, K.: Measurement and calculation of optical band gap of chromium aluminum oxide films. *Jpn. J. Appl. Phys.* **39**, 4820 (2000)
- Kim, M., Lee, B.Y., Ham, H.C., Han, J., Nam, S.W., Lee, H.-S., Park, J.H., Choi, S., Shin, Y.: Facile one-pot synthesis of tungsten oxide (WO_{3-x}) nanoparticles using sub and supercritical fluids. *J. Supercrit. Fluids* **111**, 8–13 (2016)
- Kumar, V.B., Mohanta, D.: Formation of nanoscale tungsten oxide structures and colouration characteristics. *Bull. Mater. Sci.* **34**, 435–442 (2011)
- Lavanya, N., Anithaa, A., Sekar, C., Asokan, K., Bonavita, A., Donato, N., Leonardi, S., Neri, G.: Effect of gamma irradiation on structural, electrical and gas sensing properties of tungsten oxide nanoparticles. *J. Alloy. Compd.* **693**, 366–372 (2017)
- Lee, K., Seo, W.S., Park, J.T.: Synthesis and optical properties of colloidal tungsten oxide nanorods. *J. Am. Chem. Soc.* **125**, 3408–3409 (2003)
- Mansoureh, G., Parisa, V.: *Synthesis of Metal Nanoparticles Using Laser Ablation Technique, Emerging Applications of Nanoparticles and Architecture Nanostructures*, pp. 575–596. Elsevier, Amsterdam (2018)
- Moradi, M., Solati, E., Darvishi, S., Dorrnian, D.: Effect of aqueous ablation environment on the characteristics of ZnO nanoparticles produced by laser ablation. *J. Cluster Sci.* **27**, 127–138 (2016)
- Mostafa, A.M., Yousef, S.A., Eisa, W.H., Ewaida, M.A., Al-Ashkar, E.A.: WO₃ quantum dot: synthesis, characterization and catalytic activity. *J. Mol. Struct.* **1185**, 351–356 (2019)
- Pankove, J.I.: *Optical Processes in Semiconductors*, 2nd edn. Courier Corporation, Chelmsford (2010)
- Petit, T., Puskar, L.: FTIR spectroscopy of nanodiamonds: Methods and interpretation. *Diam. Relat. Mater.* (2018). <https://doi.org/10.1016/j.diamond.2018.08.005>
- Petit, T., Puskar, L., Dolenko, T., Choudhury, S., Ritter, E., Burikov, S., Laptinskiy, K., Brzustowski, Q., Schade, U., Yuzawa, H.: Unusual water hydrogen bond network around hydrogenated nanodiamonds. *J. Phys. Chem. C* **121**, 5185–5194 (2017)
- Popov, A., Zholobak, N., Balko, O., Balko, O., Shcherbakov, A., Popova, N., Ivanova, O., Baranchikov, A., Ivanov, V.: Photo-induced toxicity of tungsten oxide photochromic nanoparticles. *J. Photochem. Photobiol. B* **178**, 395–403 (2018)
- Ragunathan, A., Krishnan, R., Kamaludeen, B.A.: Stability of tungsten oxide nanoparticles in different media. *J. Chem. Res.* **39**, 622–626 (2015)
- Schieder, M., Lunkenbein, T., Martin, T., Milius, W., Auffermann, G., Breu, J.: Hierarchically porous tungsten oxide nanotubes with crystalline walls made of the metastable orthorhombic polymorph. *J. Mater. Chem. A* **1**, 381–387 (2013)
- Sekhon, J.S., Malik, H.K., Verma, S.: Tailoring surface plasmon resonance wavelengths and sensoric potential of core-shell metal nanoparticles. *Sens. Lett.* **11**, 512–518 (2013a)
- Sekhon, J.S., Malik, H.K., Verma, S.: DDA simulations of noble metal and alloy nanocubes for tunable optical properties in biological imaging and sensing. *RSC adv.* **3**, 15427–15434 (2013b)
- Shah, M., Muzyyan, N., Hazratbal, S.: A novel approach for the synthesis of tungsten trioxide nanostructures. *J. King Abdulaziz Univ. Sci.* **21**, 109–115 (2009)
- Shenderova, O., Panich, A., Moseenkov, S., Hens, S., Kuznetsov, V., Vieth, H.-M.: Hydroxylated detonation nanodiamond: FTIR, XPS, and NMR studies. *J. Phys. Chem. C* **115**, 19005–19011 (2011)
- Solati, E., Dorrnian, D.: Comparison between silver and gold nanoparticles prepared by pulsed laser ablation in distilled water. *J. Cluster Sci.* **26**, 727–742 (2015)
- Solati, E., Dorrnian, D.: Nonlinear optical properties of the mixture of ZnO nanoparticles and graphene nanosheets. *Appl. Phys. B* **122**, 76 (2016a)
- Solati, E., Dorrnian, D.: Effect of temperature on the characteristics of ZnO nanoparticles produced by laser ablation in water. *Bull. Mater. Sci.* **39**, 1677–1684 (2016b)
- Stehlik, S., Glatzel, T., Pichot, V., Pawlak, R., Meyer, E., Spitzer, D., Rezek, B.: Water interaction with hydrogenated and oxidized detonation nanodiamonds—Microscopic and spectroscopic analyses. *Diam. Relat. Mater.* **63**, 97–102 (2016)
- Supothina, S., Seeharaj, P., Yoriya, S., Sriyudthsak, M.: Synthesis of tungsten oxide nanoparticles by acid precipitation method. *Ceram. Int.* **33**, 931–936 (2007)
- Tauc, J., Menth, A.: States in the gap. *J. Non-Cryst. Solids* **8**, 569–585 (1972)
- Tiwari, A., Gong, S.: Electrochemical synthesis of Chitosan-co-polyaniline/WO₃·nH₂O composite electrode for amperometric detection of NO₂ Gas. *Electroanal.: Int. J. Devot. Fundam. Pract. Asp. Electroanal.* **20**, 1775–1781 (2008)
- Viezbicke, B.D., Patel, S., Davis, B.E., Birnie, D.P.: Evaluation of the Tauc method for optical absorption edge determination: ZnO thin films as a model system. *physica status solidi (b)* **252**, 1700–1710 (2015)

- Wang, Y., Wang, X., Xu, Y., Chen, T., Liu, M., Niu, F., Wei, S., Liu, J.: Simultaneous synthesis of WO_3-x quantum dots and bundle-like nanowires using a one-pot template-free solvothermal strategy and their versatile applications. *Small* **13**, 1603689 (2017)
- Wasmi, B.A., Al-Amiery, A.A., Kadhum, A.A.H., Mohamad, A.B.: Novel approach: tungsten oxide nanoparticle as a catalyst for malonic acid ester synthesis via ozonolysis. *J. Nanomater.* **2014**, 2 (2014)
- Yahiaoui, K., Kerjja, T., Malek, S.: Phase explosion in tungsten target under interaction with Nd: YAG laser tripled in frequency. *Surf. Interface Anal.* **42**, 1299–1302 (2010)
- Yamazaki, S., Shimizu, D., Tani, S., Honda, K., Sumimoto, M., Komaguchi, K.: Effect of dispersants on photochromic behavior of tungsten oxide nanoparticles in methylcellulose. *ACS Appl. Mater. Interfaces* **10**, 19889–19896 (2018)
- Zamiranvari, A., Solati, E., Dorrnian, D.: Effect of CTAB concentration on the properties of graphene nanosheet produced by laser ablation. *Opt. Laser Technol.* **97**, 209–218 (2017)
- Zhan, Y., Liu, Y., Liu, Q., Liu, Z., Yang, H., Lei, B., Zhuang, J., Hu, C.: Size-controlled synthesis of fluorescent tungsten oxide quantum dots via one-pot ethanol-thermal strategy for ferric ions detection and bioimaging. *Sens. Actuators B Chem.* **255**, 290–298 (2018)
- Zhao, Z., Bai, Y., Ning, W., Fan, J., Gu, Z., Chang, H., Yin, S.: Effect of surfactants on the performance of 3D morphology W18O49 by solvothermal synthesis. *Appl. Surf. Sci.* **471**, 537–544 (2019)
- Zheng, H., Ou, J.Z., Strano, M.S., Kaner, R.B., Mitchell, A., Kalantar-zadeh, K.: Nanostructured tungsten oxide—properties, synthesis, and applications. *Adv. Func. Mater.* **21**, 2175–2196 (2011)

Publisher's Note Springer Nature remains neutral with regard to jurisdictional claims in published maps and institutional affiliations.